ELSEVIER

Applied Ocean Research 23 (2001) 83–91

Applied Ocean Research

www.elsevier.com/locate/apor

# On the dynamic compression of risers: an analytic expression for the critical load

J.A.P. Aranha[a,*], M.O. Pinto[a], R.M.C. da Silva[b]

[a]*Department of Naval Engineering, USP, CP61548, Sao Paulo, Brazil*
[b]*E and P, Petrobras, Rio de Janeiro, Brazil*

Received 20 June 2000; revised 20 March 2001

**Abstract**

A riser is anchored at the floating system in a quasi-vertical configuration, the angle between the tangent and the vertical line at the top end being, in general, small. As a consequence, the static tension at the touchdown point is also small and the riser usually becomes dynamically compressed when excited by a moderate sea state. In this paper, a physical argument, coupled with a simple model for the quasi-steady buckling of a infinitely long *curved beam*, allows one to obtain a simple estimative for the *critical load*, namely, the maximum value of the compression permitted in a given situation. In this context, the total tension should follow nearly the harmonic result predicted by the algebraic expression derived in Aranha and Pinto [Dynamic tension in risers and mooring lines: an algebraic approximation for harmonic excitation (2001), submitted] but *saturated*, in the compressed part, at this critical load, a conclusion suggested by experimental results due to Andrade [EPSUP (1993)]. Comparison with numerical results, obtained from nonlinear time domain programs, indicate a fairly good agreement, in the sense that the numerically determined tensions tend, indeed, to 'saturate' in compression around the estimated critical load. 

*Keywords*: Dynamic compression; Critical load; Saturate

## 1. Introduction

In this work a cable structure, anchored at the top end of a floating system and resting on the sea floor at the other end, is considered. The cable is statically subjected to its own submerged weight and, possibly, to an horizontal ocean current; furthermore, it is supposed to be also excited dynamically by a harmonic motion imposed on its top end. Let $T(s)$ be the effective static tension on the cable, with $s = 0$ at the touchdown point and $s = l$ at the top, where $l$ is the suspended length, and $T_D(s)$ be the amplitude of the dynamic tension. The situation where $T_D(s) > T(s)$ is not uncommon, mainly for the almost vertical static configuration used for risers: in this case, the static tension in the vicinity of the touchdown point is very small and it can be easily surpassed by the dynamic tension. Since the dynamic tension changes cyclically in time, the condition $T_D(s) > T(s)$ implies that the cable becomes compressed into part of the wave cycle and the cable is then said to be *dynamically compressed*. The intention of this work is to study this problem.

In the strict sense of the word, a cable does not have a bending stiffness (EJ = 0) and so it cannot support any compressive load: in the 'compressed zone' the dynamic tension adjusts its value in such a way that the total tension $T_{TOTAL}(s,t)$ remains zero during this part of the wave cycle. The cable then slackens and folds (infinite curvature) but it recovers its tightness as soon as the total tension becomes positive again. This qualitative description has a strong experimental support. For example, as shown in numerous experiments done by Andrade [1], the total tension at the suspended end of a chain can be approximated by $T_{TOTAL}(l,t) = (1/2)[1 + \text{sign}(T(l) + T_D(l)\cos(\omega t))](T(l) + T_D(l)\cos(\omega t))$, with $T_D(l)$ being the *harmonic amplitude* of the dynamic tension, see Ref. [3]; this expression indicates not only the *saturation* when $T(l) + T_D(l)\cos(\omega t) < 0$ but also a strict *harmonic behavior* when $T_{TOTAL}(l,t) = T(l) + T_D(l)\cos(\omega t) > 0$. Fig. 3.1b in Ref. [3], extracted from Ref. [1], is typical: it shows the adequacy of the proposed expression for $T_{TOTAL}(l,t)$ while displaying clearly the *saturation region* where the tension remains zero.

A riser has a bending stiffness (EJ ≠ 0) and so it can

* Corresponding author. Address: Department of Naval and Ocean Engineering, Cidade University, EPSUP, CEP 05508-900, Sao Paulo, Brazil. Tel.: +55-11-3818-5340; fax: +55-11-3818-5717.
*E-mail address:* japaran@usp.br (J.A.P. Aranha).

0141-1187/01/$ - see front matter 
PII: S0141-1187(01)00009-8

**Nomenclature**

List of symbols

| | |
|---|---|
| $q$ | submerged weight per unit of length (N m$^{-1}$) |
| $m$ | mass per unit of length (kg m$^{-1}$) |
| $m_a$ | added mass per unit of length (kg m$^{-1}$) |
| EJ | flexural stiffness (N m$^2$) |
| EA | axial stiffness (N) |
| $T_0$ | static tension (N) |
| $T_D$ | dynamic compression in the saturated condition (N) |
| $P = T_D - T_0$ | total compressive load on the riser (N) |
| $y(s)$ | static displacement in the transversal direction (m) |
| $y'' = q/T_0 = \chi$ | static curvature (m$^{-1}$) |
| $V(s) = y(s) + v(s)$ | total displacement in the transversal direction (m) |
| $v(s)$ | buckling mode (m) |
| $2\pi/k$ | wavelength of straight beam buckling mode, see Eq. (2.1b) (m) |
| $\beta_{cr}(\chi)$ | root of Eq. (2.6) |
| $P_{cr}(\chi)$ | buckling load, see Eq. (2.7) (N) |
| $\lambda_{cr}(\chi)$ | wavelength of the buckled mode, see Eq. (2.7) (m) |

support some compression. By analogy with the cable result, it is expected here the existence of a positive *critical load* $P_{cr}$ that would play for the riser the same role played by the load $P_{cr} = 0$ in the cable case. In particular, it is also expected, by extension of the observed experimental results for the cable that the total tension in the riser should be given by an expression of the form

$$T_{TOTAL}(s,t) = \frac{1}{2}[1 + \text{sign}(T(s) + T_D(s)\cos\omega t + P_{cr})](T(s) + T_D(s)\cos\omega t) - \frac{1}{2}[1 - \text{sign}(T(s) + T_D(s)\cos\omega t + P_{cr})]P_{cr} \quad (1.1)$$

with $T_D(s)$ being, again, the *harmonic amplitude* of the dynamic tension. The basic result in Ref. [3] was the derivation of an algebraic approximation for this amplitude.

The main objective of the present work is to obtain an estimative of the critical load $P_{cr}$; in reality, as it will be seen, this critical value changes along the suspended length, once it is a function of the local static curvature, and so $P_{cr} = P_{cr}(s)$. The total tension should *saturate* at this critical value ($T_{TOTAL}(s,t) \geq -P_{cr}(s)$), a result that does have importance in itself: in one hand, since $P_{cr}(s)$ is the maximum possible compression in a *flexible riser*, one may confront this value with the maximum allowable compression, in general specified by the manufacturer, to check whether or not the riser would be in safe condition while in operation; on the other hand, this critical value can define the maximum permissible dynamic tension in a *steel riser* in order to avoid the large curvatures (buckling) that may appear in the *saturated region*, where $T_{TOTAL}(s,t) = -P_{cr}$.

As discussed in Ref. [3], the analytic estimate of $P_{cr}$ has an even greater importance for a single reason: in general, numerical results seem to be not very precise in the vicinity of the critical load, in such a way that relatively large compressions are sometimes numerically observed in a cable (EJ = 0) despite the fact that these structural elements cannot support any compression; see, for example, Fig. 3.2b in Ref. [3]. By extension, again, one should expect possible numerical problems around the 'saturation region' of a riser (EJ $\neq$ 0) and a difficulty to interpret the results if a reference value is not known. In other words: if the critical load $P_{cr}$ is not known a priori it may become awkward to distinguish, in the numerical output, the real physical response from the numerical ill behavior.

This work has been organized in the following way: in Section 2 a mathematical model is proposed and a closed form expression for the critical load is obtained; in Section 3 the derived expression for $P_{cr}$ is compared with some numerical results, in order to check its adherence to the observed numerical trend and to qualify, whenever necessary, the detected numerical ill behavior. Section 4 presents the conclusions.

## 2. Mathematical model: estimative of the critical load

Consider an infinitely long straight beam with bending stiffness EJ and a wave mode $v(x) = A\sin(kx)$. The classical *Euler buckling load* is then given by

$$P_{cr} = EJk^2. \quad (2.1a)$$

Obviously, the basic problem is the yet undetermined wave number $k$ but the following argument can shed some light on this point: if the beam is dynamically excited at the frequency $\omega$ it naturally assumes a waveform with wave number $k$ determined from the beam dispersion relation, namely

$$k^2 = \sqrt{\frac{m + m_a}{EJ}}\,\omega, \quad (2.1b)$$

where $m$ is the mass per unit of length and $m_a$ is the added mass. It seems reasonable to assume that the beam will choose this wave number to buckle and, in this context, the critical load can be estimated by Eqs. (2.1a) and (2.1b). However, the riser is a *curved beam* and the critical load is influenced by the curvature. The proper model for this case is derived in the next item.

### 2.1. Eigenvalue problem for a curved beam

The equilibrium equation for a beam with bending stiffness EJ, subjected to a *compressive load P* and to a lateral

load $q$ is given by

$$\mathrm{EJ}\frac{\mathrm{d}^4V}{\mathrm{d}s^4} + P\frac{\mathrm{d}^2V}{\mathrm{d}s^2} = q. \tag{2.2a}$$

For a *straight beam* ($q = 0$) the solution of Eq. (2.2a) can be expressed in the form

$$V(s) = \mathrm{Imag}\{A\mathrm{e}^{\mathrm{i}ks}\} = A\sin(ks) \tag{2.2b}$$

that placed in Eq. (2.2a) with $q = 0$ gives the Euler buckling load (2.1a). The intention here is to obtain a solution of Eq. (2.2a) that tends to Eq. (2.2b) in the limit $q \to 0$. For example, if $T_0$ is the static tension in the vicinity of the touchdown point, the local static curvature[1] is given by $\chi = q/T_0$ and if $-T_\mathrm{D}$ is the 'dynamic tension', one can write

$$V(s) = v(s) + y(s), \qquad \frac{\mathrm{d}^2y}{\mathrm{d}s^2} = -\frac{q}{T_0}, \qquad P = T_\mathrm{D} - T_0. \tag{2.2c}$$

In Eq. (2.2c) the force $P$ is the riser total compressive load in the saturation region and the equilibrium equation (2.2a) is reduced to ($T_\mathrm{D} > 0$ means dynamic *compression*)

$$\mathrm{EJ}\frac{\mathrm{d}^4v}{\mathrm{d}s^4} + P\frac{\mathrm{d}^2v}{\mathrm{d}s^2} = T_\mathrm{D}\frac{q}{T_0}. \tag{2.3a}$$

The inertia term is absent in this model: the dynamic tension is assumed here to adjust its value in such a way that the total compression saturates at the critical load; for example, $T_\mathrm{D} = T_0$ for a cable (EJ = 0) in order that the compressive load 'saturates' at the critical load $P_\mathrm{cr} = 0$. The equilibrium equation (2.3a) should be coupled with the *geometric compatibility equation* for the axial deformation (see, for instance, Eq. (4.1b) in Ref. [3])

$$-\frac{T_\mathrm{D}}{EA} = \frac{\mathrm{d}u(s)}{\mathrm{d}s} + \frac{q}{T_0}v(s). \tag{2.3b}$$

The functions $\{v(s); u(s)\}$ should satisfy the boundary conditions consistent with the straight beam problem, in order that Eq. (2.2b) be recovered in the limit $q \to 0$, and so

$$v(0) = v(\pi/k) = v''(0) = v''(\pi/k) = 0, \qquad u(0) = u(\pi/k). \tag{2.3c}$$

Introducing the auxiliary variables

$$\beta^2 = \frac{P}{k^2\mathrm{EJ}}, \qquad \chi = \frac{q}{T_0}. \tag{2.4a}$$

Eqs. (2.3a) and (2.3b) can be written in the form ($\bar{s} = ks$)

$$\frac{\mathrm{d}^4v}{\mathrm{d}\bar{s}^4} + \beta^2\frac{\mathrm{d}^2v}{\mathrm{d}\bar{s}^2} = T_\mathrm{D}\chi\frac{1}{k^4\mathrm{EJ}} = f, \qquad -\frac{T_\mathrm{D}}{\mathrm{EA}} = k\frac{\mathrm{d}u(\bar{s})}{\mathrm{d}\bar{s}} + \chi v(\bar{s}) \tag{2.4b}$$

with boundary conditions

$$v(0) = v(\pi) = 0, \qquad v''(0) = v''(\pi) = 0, \qquad u(0) = u(\pi). \tag{2.4c}$$

Integrating the geometric compatibility equation (2.4b) in the interval $(0;\pi)$ one obtains

$$-f = \frac{\mathrm{EA}}{\pi}\chi^2\frac{1}{k^4\mathrm{EJ}}\int_0^\pi v(\bar{s})\,\mathrm{d}\bar{s}$$

and introducing the parameter (see Eq. (2.1b))

$$\gamma(\chi) = \left(\frac{\pi}{2}\right)^2\chi\sqrt{\frac{\mathrm{EA}}{k^4\mathrm{EJ}}} = \left(\frac{\pi}{2}\right)^2\chi\sqrt{\frac{\mathrm{EA}}{m + m_\mathrm{a}}}\frac{1}{\omega}. \tag{2.5a}$$

Eq. (2.4b) is reduced to

$$\frac{\mathrm{d}^4v}{\mathrm{d}\bar{s}^4} + \beta^2\frac{\mathrm{d}^2v}{\mathrm{d}\bar{s}^2} = f, \qquad -\frac{1}{\gamma^2(\chi)}\left(\frac{\pi}{2}\right)^5 f = \frac{1}{2}\int_0^\pi v(\bar{s})\,\mathrm{d}\bar{s}. \tag{2.5b}$$

Before the solution of Eqs. (2.4c), (2.5a) and (2.5b) is presented it seems worthwhile to establish a relation between the parameter $\gamma(\chi)$ and the parameter $\Lambda$, first introduced by Irvine and Caughey [4] in the dynamic of cables; see Eq. (2.3c) in Ref. [3] for the definition of $\Lambda$. In fact, if $\lambda = 2\pi/k$ is the wavelength, the parameter $\Lambda$ can be written as

$$\Lambda = \frac{q\lambda/2}{T_0}\left(\frac{\mathrm{EA}}{T_0}\right)^{1/2}$$

and then

$$\gamma(\chi) = \frac{1}{8}\frac{\lambda}{\lambda_\mathrm{f}}\Lambda,$$

where $\lambda_\mathrm{f} = (\mathrm{EJ}/T_0)^{1/2}$ is the *flexural length*, see Ref. [2].

The eigenvalue problems (2.4c), (2.5a) and (2.5b) have a non-trivial solution if and only if $\beta = \beta_\mathrm{cr}(\chi)$ with $\beta_\mathrm{cr}(\chi)$ being the smallest root of the *characteristic equation*

$$\tan\alpha = \alpha + \frac{\alpha^3}{3} - \frac{\alpha^5}{\gamma^2(\chi)}, \qquad \alpha = \frac{\beta_\mathrm{cr}(\chi)\pi}{2}. \tag{2.6}$$

Observing that $\tan\alpha = \alpha + \alpha^3/3 + 2\alpha^5/15$ when $\alpha \ll 1$ it is easy to check that $\tan\alpha > \alpha + \alpha^3/3 - \alpha^5/\gamma^2$ when $0 \le \alpha < \pi/2$ ($0 \le \beta < 1$); the smallest root $\alpha$ of Eq. (2.6) is then in the interval $\pi/2 \le \alpha < 3\pi/2$ ($1 \le \beta_\mathrm{cr}(\chi) < 3$). In the limit $\chi \to 0$ ($\gamma \to 0$; straight beam) the right-hand side of Eq. (2.6) tends to $-\infty$ and so $\alpha = \pi/2$ or $\beta_\mathrm{cr}(0) = 1$; in this limit the Euler critical load (2.1a) is recovered, see also Eq. (2.4a). The root $\alpha$ of Eq. (2.6) increases monotonically with $\chi$, it is equal to $\pi$ ($\beta_\mathrm{cr} = 2$) when $\gamma/\pi = 1.517$ and tends to the value $3\pi/2(1 - 0.0055)$ in the limit when $\chi \to \infty$ ($\beta_\mathrm{cr}(\infty) = 2.984$). This result is summarized and further elaborated in the next item.

### 2.2. Critical load and related parameters

The critical load $P_\mathrm{cr}(\chi)$, the *wave number* $k_\mathrm{cr}(\chi)$ and the *wavelength* $\lambda_\mathrm{cr}(\chi) = 2\pi/k_\mathrm{cr}(\chi)$ of the related wavemode are

[1] The influence of the bending stiffness in the vicinity of the touchdown point has been ignored here: the thin bending boundary layer should not affect the buckling load. The numerical results of Section 3 confirm this assumption.

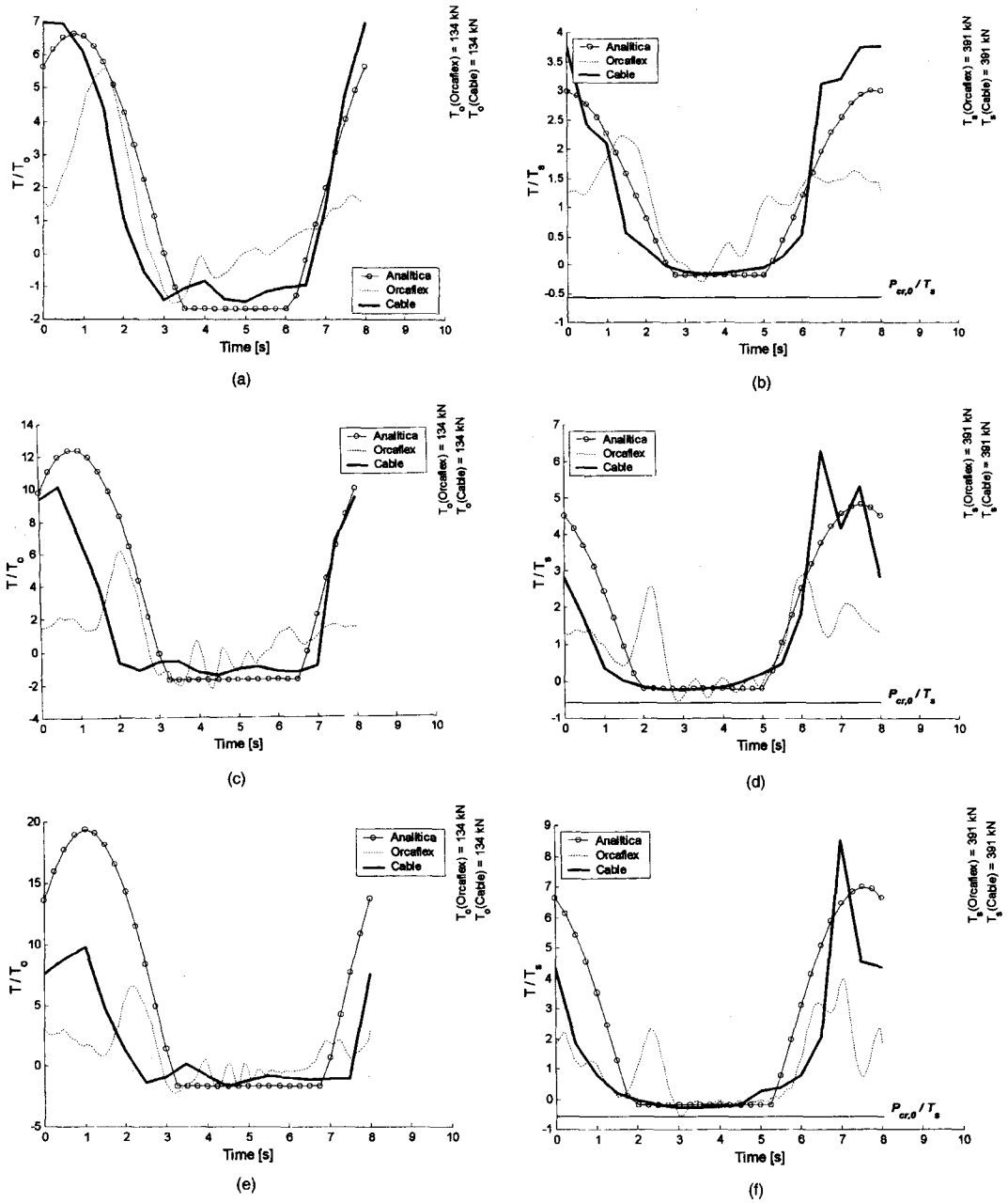


Fig. 1. (a) Total tension at the TDP. Steel riser, ($P = 8$ s; $A = 4$ m). (-O-) Theory (1.1) and (2.7); (—) Cable; (- - -) Orcaflex. (b) Total tension at the TOP. Steel riser, ($P = 8$ s; $A = 4$ m). (-O-) Theory (1.1) and (2.7); (—) Cable; (- - -) Orcaflex. (c) Total tension at the TDP. Steel riser, ($P = 8$ s; $A = 6$ m). (-O-) Theory (1.1) and (2.7); (—) Cable; (- - -) Orcaflex. (d) Total tension at the TOP. Steel riser, ($P = 8$ s; $A = 6$ m). (-O-) Theory (1.1) and (2.7); (—) Cable; (- - -) Orcaflex. (e) Total tension at the TDP. Steel riser, ($P = 8$ s; $A = 8$ m). (-O-) Theory (1.1) and (2.7); (—) Cable; (- - -) Orcaflex. (f) Total tension at the TOP. Steel riser, ($P = 8$ s; $A = 8$ m). (-O-) Theory (1.1) and (2.7); (—) Cable; (- - -) Orcaflex.

then given by (see Eqs. (2.1b) and (2.4a))

$$k_{cr}(\chi) = \beta_{cr}(\chi)\left(\frac{(m + m_a)\omega^2}{EJ}\right)^{1/4},$$

$$\lambda_{cr}(\chi) = \frac{2\pi}{k_{cr}(\chi)} = \frac{2\pi}{\beta_{cr}(\chi)}\left(\frac{EJ}{(m + m_a)\omega^2}\right)^{1/4}, \tag{2.7}$$

$$P_{cr}(\chi) = EJk_{cr}^2(\chi) = \beta_{cr}^2(\chi)\sqrt{(m + m_a)EJ}\omega,$$

where $\chi = \chi(s)$ is the *local static curvature* at the riser's section $s$ and $1 \leq \beta_{cr}(\chi) < 2.984$ is the root of the characteristic equations (2.5a) and (2.6). The only purpose in being specific about the touchdown point was to make more direct the argument, the final result being general.

The *local* character of the buckling mode can be easily visualized if it is recalled that a riser is relatively 'curved' near the touchdown point but it has a 'stretched' configuration at the suspended end. Formally, this local character is a

consequence of the fact that the wavelength $\lambda_{cr}(\chi)$ of the buckling mode is, in general, much smaller than the suspended length $l$ of the riser, as shown below, and so the buckling mode can always assume its local wavelength.

Table 1 displays the main buckling parameters of the steel riser defined in Table 3.2 of Ref. [3]. The water depth is $h = 840$ m and the static configuration is defined by the angle $\theta_S = 70^\circ$ with the horizontal; $(T_0; T_S)$ are the static tension at the TDP and TOP, respectively.

At the touchdown point (TDP) the curvature is so large that the limit value $\beta_{cr}(\infty) = 2.984$ is almost reached irrespective of the wave period; in this case the critical load decreases linearly with the wave frequency. At the *suspended end* (TOP) the riser is relatively stretched and the value of $\beta_{cr}$ changes with the wave period; however, the decrease of $\beta_{cr}$ with $\omega$ is attenuated in the final expression (2.7) of the critical load, that contains also an increasing factor with $\omega$.

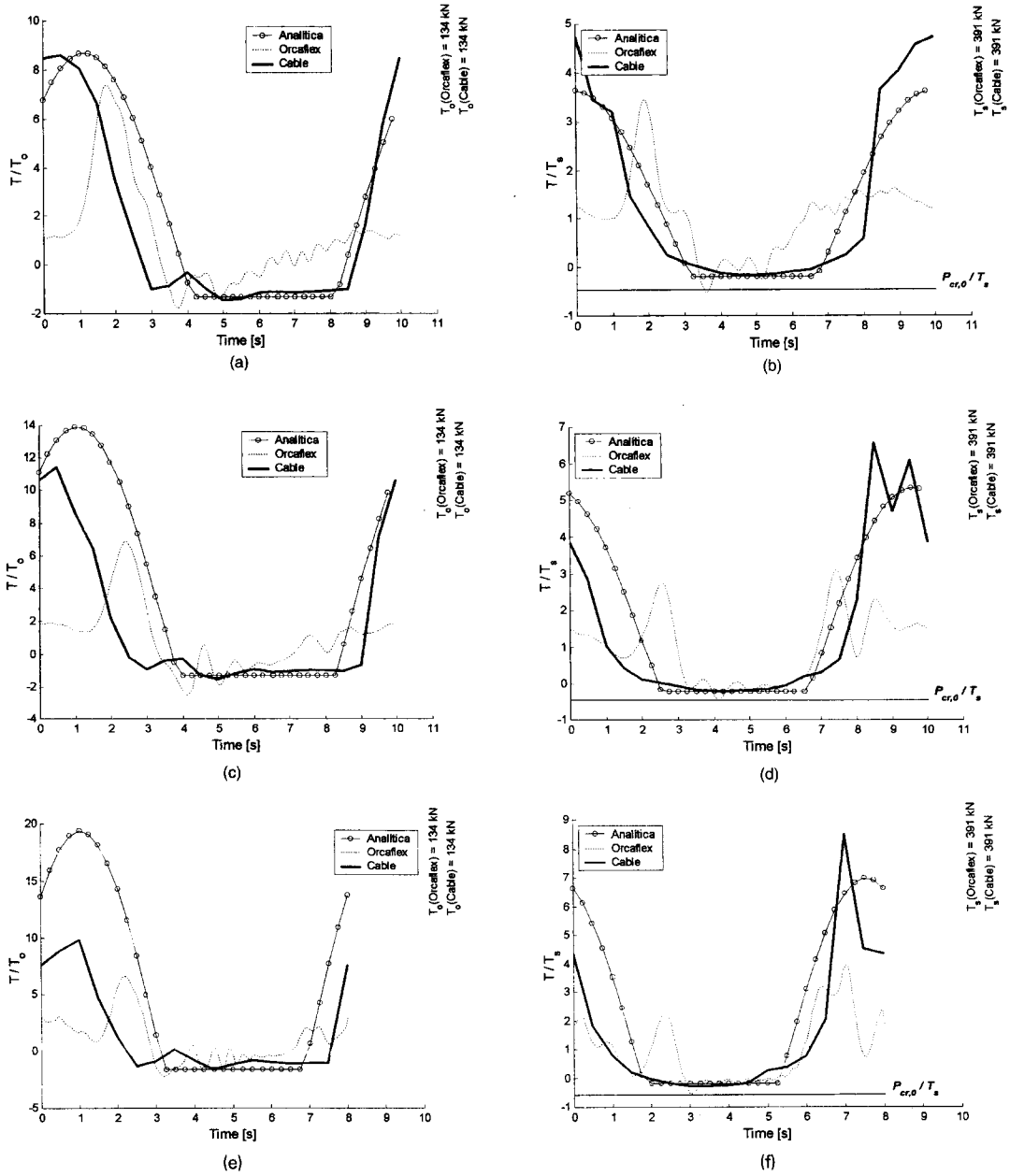


Fig. 2. (a) Total tension at the TDP. Steel riser, ($P = 10$ s; $A = 6$ m). (-O-) Theory (1.1) and (2.7); (—) Cable; (- - -) Orcaflex. (b) Total tension at the TOP. Steel riser, ($P = 10$ s; $A = 6$ m). (-O-) Theory (1.1) and (2.7); (—) Cable; (- - -) Orcaflex. (c) Total tension at the TDP. Steel riser, ($P = 10$ s; $A = 8$ m). (-O-) Theory (1.1) and (2.7); (—) Cable; (- - -) Orcaflex. (d) Total tension at the TOP. Steel riser, ($P = 10$ s; $A = 8$ m). (-O-) Theory (1.1) and (2.7); (—) Cable; (- - -) Orcaflex.

The results of Table 1 can be useful to check some features of the proposed model: first, given the relatively large spread of values in the column $P_{cr,0}/T_0$, it seems possible to detect, in the numerical simulations, the variation of the 'saturation' load with the wave period; second, by observing the difference between $\beta^2_{cr,0}$ and $\beta^2_{cr,s}$, it also seems possible to observe numerically the influence of the static curvature on the critical load. These points are explored in Section 3.

In a steel riser the non-compression condition $T_D < T_0$ is usually imposed to avoid excessive curvature; Table 1 indicates that the milder condition $T_D < 2T_0$ can be taken instead to avoid buckling. For a *flexible riser* with EJ = 9.84 kN m$^2$; $m + m_a = 104$ kg m$^{-1}$, see Table 3.2 of Ref. [3], one has $P_{cr} \leq 7$ kN when the wave period is larger than 8 s, indicating that the *maximum* possible compression is in fact very small and independent of the wave amplitude. Both results disclose the practical importance that Eq. (2.7) should have in the design of a riser.

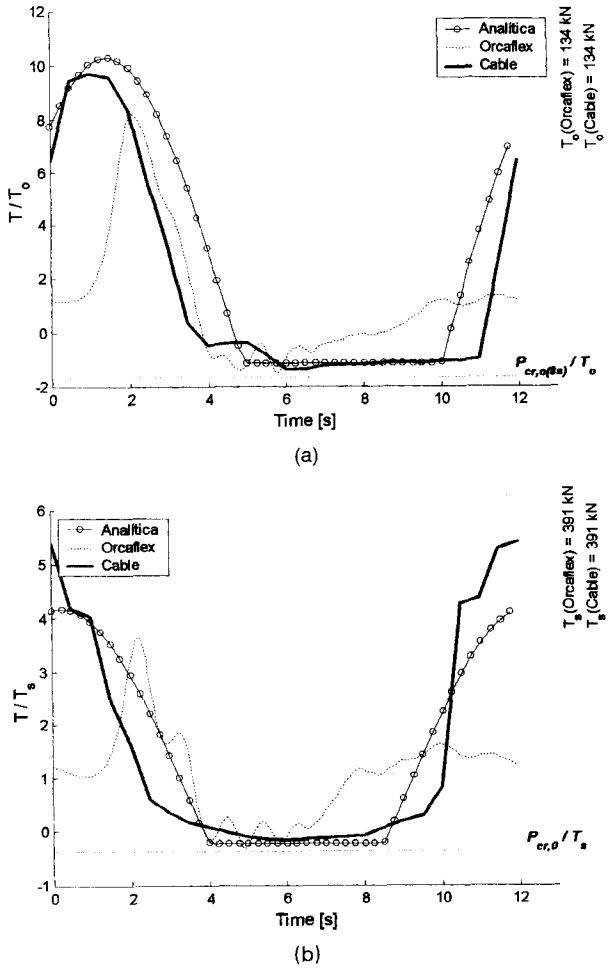


Fig. 3. (a) Total tension at the TDP. Steel riser, ($P = 12$ s; $A = 8$ m). (-O-) Theory (1.1) and (2.7); (—) Cable; (- - -) Orcaflex. (b) Total tension at the TOP. Steel riser, ($P = 12$ s; $A = 8$ m). (-O-) Theory (1.1) and (2.7); (—) Cable; (- - -) Orcaflex.

Table 1
Parameters of the buckling mode. Steel riser (EJ = 9241 kN; $m + m_a = 108.6$ kg m$^{-1}$; $q = 0.307$ kN m$^{-1}$). Static configuration: $\theta_S = 70^\circ$; $h = 840$ m; $l = 1196$ m

| Period (s) | TDP | | | TOP | | |
|---|---|---|---|---|---|---|
| | $\lambda_{cr,0}/l$ (%) | $\beta^2_{cr,0}$ | $P_{cr,0}/T_0$ | $\lambda_{cr,S}/l$ (%) | $\beta^2_{cr,S}$ | $P_{cr,S}/T_S$ |
| 8 | 0.54 | 8.90 | 1.65 | 0.96 | 2.85 | 0.18 |
| 10 | 0.60 | 8.90 | 1.33 | 0.92 | 3.87 | 0.20 |
| 12 | 0.66 | 8.90 | 1.10 | 0.87 | 5.11 | 0.22 |

## 3. Numerical results

Both the steel riser (SR) and the *flexible riser* (FR) defined in Table 3.2 of Ref. [3] have been numerically simulated by the programs CABLE and ORCAFLEX under a variety of conditions, summing a total of 36 simulations for each riser. The results to be shown here are typical although the choice was not arbitrary: the cases where dynamic compression occurred also at the top end have been singled out since they display better than the influence of the local curvature on the critical load. By the same reason, the results from the steel riser were selected, since the relation $P_{cr,0}/T_0$ is larger there and can be more easily seen in the figures. At the end of this section an example of a flexible riser in random excitation is discussed.

All results to be shown refer to the same static configuration: a steel riser placed in a water depth $h = 840$ m with an angle $\theta_S = 70^\circ$ with the horizontal at the top, see Table 1. A circular harmonic motion at the suspended end was imposed to the riser and the following simulations, characterized by the period $P$ and amplitude $A$, will be discussed here: ($P = 8$ s; $A = 4$, 6, 8 m), ($P = 10$ s; $A = 6$, 8 m) and ($P = 12$ s; $A = 8$ m). For example, the case ($P = 12$ s; $A = 6$ m) was not chosen since the total tension was always positive at the suspended end and no compression could be

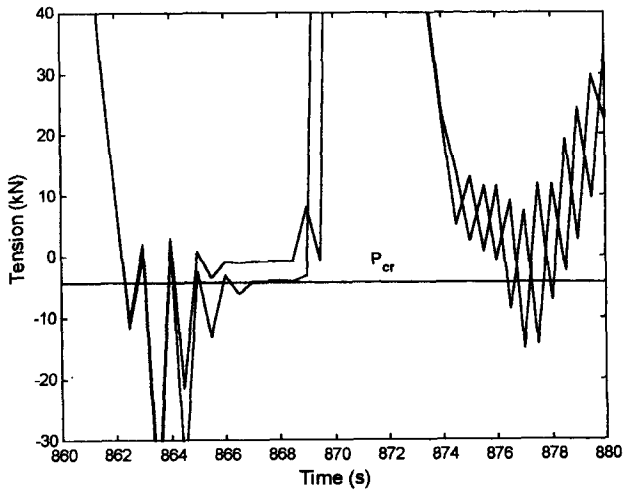


Fig. 4. Flexible riser under random excitation. $\theta_S = 85^\circ$. (- - -) EJ = 9.8 kN m$^2$; (—) EJ = 0 (Orcaflex).

observed. Figs. 1a–f, 2a–d and 3a,b present the comparison between the *total tension* obtained from the programs CABLE, ORCAFLEX and the analytic solution (1.1), with $T_D(s)$ computed from the algebraic approximation derived in Ref. [3]; in accordance with the notation introduced in Table 1, ($P_{cr,0}$; $T_0$) represent, respectively, the critical load and the static tension at the TDP and ($P_{cr,S}$; $T_S$) the same values at the TOP.

Fig. 1a,b refers to the case ($P = 8$ s; $A = 4$ m) at the TDP and TOP. At the TDP a relatively fair adherence between the three results is observed, although the Orcaflex result seems to be off around the saturation region; however, the Cable result shows a tendency for saturation at the level predicted theoretically. The comparison at the TOP shows a more wild discrepancy between the numerical results, as already pointed in Ref. [3], although the Cable result is somewhat closer to the analytic expression (1.1); furthermore, the saturation of the total tension in Cable's result, at the level predicted by Eq. (2.7), is now quite evident, see also Table 1. In the same figure the line $P_{cr,0}/T_S$ gives the saturation value at the TDP, showing the difference caused by the local static curvature of the riser on the critical load. Apparently Eq. (2.7) is able to predict well how the critical load is modified along the riser, a result supported by the other numerical simulations to be discussed below.

Fig. 1c,d refers to the case ($P = 8$ s; $A = 6$ m). Cable's result shows a clear saturation at the theoretical level but Orcaflex result displays a 'wavier' tendency around the saturation value. This behavior is similar to the one observed for a cable, see Ref. [3], where the tension oscillates around the critical load $P_{cr} = 0$ in spite of the fact that no compression can be supported then. At the TOP the saturation of Cable's result is also clear and the wavy tendency of Orcaflex result can also be observed; the difference between $P_{cr,S}$ and $P_{cr,0}$ is again evident.

Again, Fig. 1e,f refers to the case ($P = 8$ s; $A = 8$ m) at the TDP and TOP. The same general comments made before also apply here but there is one point that must be stressed: if the cases ($P = 8$ s; $A = 4$ m) and ($P = 8$ s; $A = 8$ m) are compared, the *maximum* total tension increases, as it should,

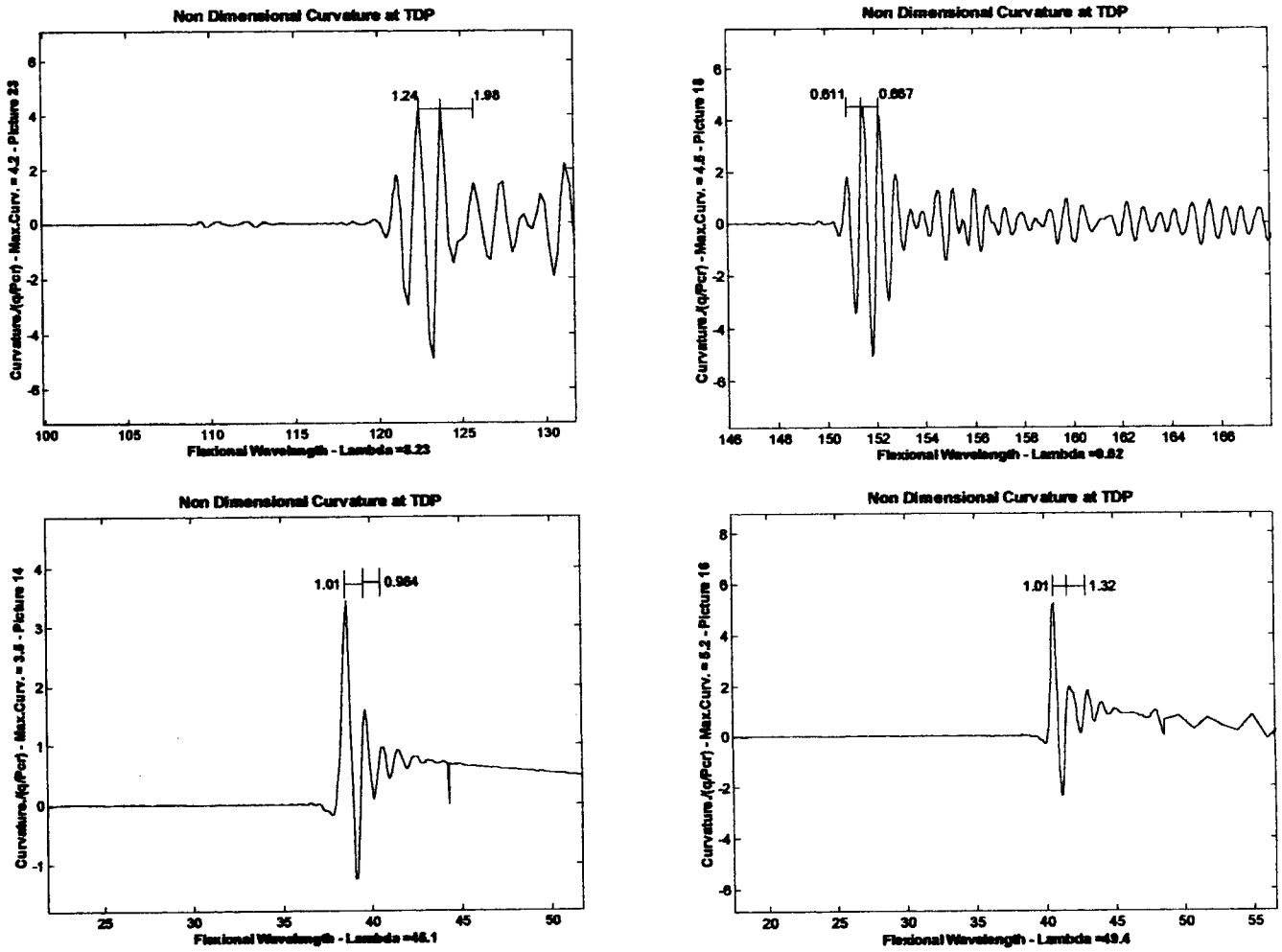


Fig. 5. Spatial variation of the dynamic curvature in the buckled region. ($\theta_S = 60^\circ$, $P = 10$ s; $A = 8$ m), left; ($\theta_S = 70^\circ$, $P = 12$ s; $A = 6$ m), right. Flexible riser (upper row), Steel riser (lower row).

with the amplitude A but the *minimum* total tension remains always at the same level, saturated at a value very close to the theoretically predicted $-P_{cr}$.

Similar comments can be made for the results displayed in Figs. 2a–d and 3a,b, the only purpose to present them here being to show that the observed agreement is in fact general, not restricted to some particular conditions. However, there is one aspect that it is worth to mentioning: the critical load changes with the wave frequency $\omega$ and it has different values in the case of Fig. 1a,c,e, where $P = 8$ s, and in Fig. 3a, where $P = 12$ s, being 1.5 times smaller in this latter situation, as indicated in the column $P_{cr,0}/T_0$ of Table 1. This result is also supported by the numerical simulations, as it can be seen in Fig. 3a: in this figure the analytic solutions (1.1) and (2.7) show the saturation of the total tension (critical load) at the period $P = 12$ s and, for the sake of comparison, the saturation corresponding to the period $P = 8$ s was also plotted, being indicated by the horizontal line with the symbol $P_{cr,0(8s)}/T_0$. Notice that the numerical results coalesce in the vicinity of the critical load at the period 12 s and not around the critical load at 8 s. The dependence of the critical load on the wave frequency seems to be well predicted by Eq. (2.7).

So far all the analysis was restricted to a harmonic excitation but it can be easily extended to a *random input* if a further assumption is made. In fact, when a random sea interacts with a floating system, the high frequency components are usually filtered out by the transfer function of the floating system, resulting in a *narrow banded* random excitation at the top of the riser. In this case, the displacement $U(t)$ imposed at the suspended end is a quasi-harmonic input of the form $U(t) = U_0(t)\cos(\omega_U t)$, with an amplitude $U_0(t)$ slowly varying in time and a frequency $\omega_U$ corresponding to the *central frequency* of the spectrum of $U(t)$. In this circumstance one should expect that the total tension should saturate at a value around the one defined by Eq. (2.7), but with the frequency $\omega_U$ in place of $\omega$.

This theoretical result has also some support from the direct numerical simulation. In Fig. 4 the time series of the total tension on a *flexible riser*, computed by ORCAFLEX, is shown. The riser, the same analyzed in Ref. [3], was placed in a turret of an actual FPSO anchored in a water depth $h = 1000$ m. The static configuration was defined by the angle $\theta_S = 85°$ with the horizontal at the top and the riser was exposed to a random sea, resulting in a displacement at the tangent direction with narrow bandwidth. Two cases have been simulated: one, with EJ = 0; the other, with the actual EJ = 9.8 kN m$^2$. The case EJ = 0 shows the usual numerical ill behavior, with the presence of negative tension, and a clear tendency to saturate at the level $P_{cr} = 0$; the case EJ = 9.8 N m$^2$ shows an overall similar behavior but now the total tension tends to be saturated at the level $-4.42$ kN, that is exactly the critical load (2.7) computed with $\omega_U$ in place of $\omega$. The proposed model seems then to be able to cope with a narrow banded random excitation.

When the total tension saturates at the critical load the riser buckles and the curvature increases along the part of the wave cycle where $T_{TOTAL}(s,t) = -P_{cr}$. The dynamic behavior of the curvature in the buckled region has a considerable importance in the riser design and, although not being the purpose of the present work, some general remarks about it can be made here. In particular, by a simple scale argument one can infer that the total curvature in the buckled region should be proportional to $q/P_{cr}$ ($\chi_{TOTAL}(s,t) \propto q/P_{cr}$), undulating in the space with a wavelength near to the critical value $\lambda_{cr}(\chi)$. These inferences are supported by the numerical results, as shown in Fig. 5: the variation in space of the curvature in the vicinity of the touchdown point is displayed in this figure, both for a *flexible riser* and for a steel riser. The curvature is normalized by the value $q/P_{cr}$ and the coordinate $s$ by $\lambda_{cr}(\chi)$ for both the flexible and steel risers: in all situations, the maximum normalized curvature is of order 5 and the undulation has a normalized wavelength of order 1, in spite of the huge difference that these parameters have for these two types of risers, since $(q/P_{cr})_{FIEX}/(q/P_{cr})_{STEEL} = 30.6$ and $(\lambda_{cr})_{STEEL}/(\lambda_{cr})_{FIEX} = 5.5$.

The question of the dynamic curvature in the buckled region will be addressed in a forthcoming work.

## 4. Conclusions

A simple expression for the critical load, the maximum total compression that a riser is able to locally withstand for an excitation with a given frequency $\omega$, was derived in this work and synthesized in Eq. (2.7). The proposed expression, when compared with numerical results, seems to cope well not only with the variation of the critical load with the frequency but also with the local static curvature of the riser; in particular, for a steel riser the critical load at the touchdown point, where the riser is relatively curved, can be more than three times larger than at the suspended end, where the riser is locally much more stretched in its static configuration.

As discussed in this work, the values of the critical parameters $\{P_{cr}; \lambda_{cr}\}$ have an importance in itself and they also command the behavior of the total curvature in the part of the wave cycle where the riser buckles, as shown in Fig. 5. The important question of the estimative of the maximum possible curvature in the buckled region was not addressed in the present work but it will be in a forthcoming paper.

Expression (1.1) for the total tension has been suggested by the experimental results due to Andrade [1]. Although it has relative support from some numerical results, see Ref. [3], it is evident that the numerical results themselves become a bit lost when the imposed amplitude (or frequency) is very large.

The interesting aspect of Eq. (1.1), well documented by the experiments, is the fact that the maximum positive tension is apparently not very much affected by the strong non-linearity (saturation of the tension) that may be occurring in the compressed part of the wave cycle; furthermore, this maximum positive tension can be relatively well estimated by the algebraic approximation derived in Ref. [3], assuming a harmonic response. The practical implication of Eq. (1.1) will be explored in the last paper of this series, which deals with the probability density function for the envelope of the dynamic tension when the cable is excited by a random wave.

## References

[1] Andrade BLR. Estudo experimental do comportamento dinâmico de linhas de amarração, Tese de Mestrado, Departamento de Engenharia Naval e Oceânica, EPUSP, 1993.

[2] Aranha JAP, Martins CA, Pesce CP. Analytical approximation for the dynamic bending moment at the touchdown point of a catenary riser. Int J Offshore Polar Engng 1997;7(4):293–300.

[3] Aranha JAP, Pinto MO. Dynamic tension in risers and mooring lines: an algebraic approximation for harmonic excitation, 2001, submitted for publication.

[4] Irvine HM, Caughey TK. The linear theory of the free vibration of a suspended cable. Philos Trans R Soc Lond A 1974;341:299–315.